J Solid State Electrochem (2004) 8: 661–667
DOI 10.1007/s10008-003-0491-8

ORIGINAL PAPER

A. V. Shlyakhtina · L. G. Shcherbakova · A. V. Knotko
A. V. Steblevskii

Study of the fluorite–pyrochlore–fluorite phase transitions in $Ln_2Ti_2O_7$ (Ln=Lu, Yb, Tm)

Received: 11 April 2003 / Accepted: 29 September 2003 / Published online: 21 February 2004

Abstract The ordering processes in $Ln_2Ti_2O_7$ (Ln = Lu, Yb, Tm) are studied by X-ray diffraction, thermal analysis, infrared absorption (IR) spectroscopy, and electrical conductivity measurements. The coprecipitation method followed by freeze-drying was used for $Ln_2Ti_2O_7$ synthesis. The region of low-temperature fluorite phase existence is 600 °C < T < 740 °C. The low-temperature fluorite–pyrochlore phase transition in $Ln_2Ti_2O_7$ takes place at ~740–800 °C. $Ln_2Ti_2O_7$ (Ln = Lu, Yb, Tm) have the structure of disordered pyrochlore with antisite Ln–Ti defects at 800 °C < T < 1,100 °C.

The high-temperature pyrochlore–fluorite transformation takes place in $Tm_2Ti_2O_7$, $Yb_2Ti_2O_7$, and $Lu_2Ti_2O_7$ in air at T > 1,600 °C. The conductivity values are $5\cdot10^{-3}$ S/cm for $Tm_2Ti_2O_7$, $6\cdot10^{-3}$ S/cm for $Yb_2Ti_2O_7$, and 10^{-2} S/cm for $Lu_2Ti_2O_7$ at 740 °C. This order–disorder transition leads to a 2 orders of magnitude conductivity growth and a 10–30 times permittivity increase in $Ln_2Ti_2O_7$ samples obtained at 1,700 °C.

Keywords Rare-earth titanates · Coprecipitation · Pyrochlore · Fluorite · Order–disorder transformation · Antisite defects · Nanocrystalline ceramics

Presented at the OSSEP Workshop "Ionic and Mixed Conductors: Methods and Processes", Aveiro, Portugal, 10–12 April 2003

A. V. Shlyakhtina (✉) · L. G. Shcherbakova
Semenov Institute of Chemical Physics, RAS, Kosygina str. 4, 119991 Moscow, Russia
E-mail: annash@chph.ras.ru
Tel.: +-09-137-83-03
Fax: +7-095-242-02-53

A. V. Knotko
Chemical Department, Moscow State University, Moscow, Russia

A. V. Steblevskii
Kurnakov Institute of General and Inorganic Chemistry, RAS, Moscow, Russia

Introduction

Pyrochlore oxides $A_2B_2O_7$ demonstrated a number of practically important properties [1], most of which deal with their high ionic conductivity resulting from the Frenkel disorder in the anion sublattice [1, 2]. It is known also that some pyrochlore materials have a tendency to order–disorder transformation at elevated temperatures, which can be modified by the incorporation of cations, differing in size or valence from the host cations of the pyrochlore structure.

Order–disorder transformation induced by composition change in $(Sc_zYb_{1-z})_2Ti_2O_7$ was investigated by Eberman et al. [2]. A decrease of the average value of the ionic radius R_A and elevated temperatures were found to cause mixed occupancy of the cation sites (antisite defects) and partial occupancy of the normally vacant oxygen site (anion Frenkel defects). This situation is similar to the disorder previously observed for $Gd_2(Zr_xTi_{1-x})_2O_7$ [1, 3]. The appearance of the antisite disorder and anion Frenkel defects is caused by allocation of the large Zr cations in Ti sites. This process is promoted also by decreasing the size difference between A and B cations in the pyrochlore structure. The high ionic conductivity of $(Sc_zYb_{1-z})_2Ti_2O_7$ and $Gd_2(Zr_xTi_{1-x})_2O_7$ gives the background for their application in fuel cells and gas sensors.

Table 1 indicates the order–disorder transformation temperatures and R_A/R_B ratio for some $A_2Zr_2O_7$ pyrochlores, where $A = Ln^{3+}$ [4, 5]. The experimental observation of the pyrochlore–fluorite transitions for a large number of pyrochlores is difficult due to the high temperatures of these transformations. For some pyrochlores with relatively low melting temperatures this transition cannot be realized. Table 2 displays the R_A/R_B ratio and melting temperatures for some rare-earth element titanates $Ln_2Ti_2O_7$ (Ln = Lu, Yb, Tm) and $Gd_2Ti_2O_7$. One can see that $Ln_2Ti_2O_7$ have the highest melting temperatures of all rare-earth titanate series and the R_A/R_B ratio for them is close to the R_A/R_B for $A_2Zr_2O_7$ (A = Gd, Sm, Nd).

Table 1 Order–disorder transformation temperatures and R_A/R_B ratio for several $Ln_2Zr_2O_7$

Compound	$R_{A(c.n.=8)}/R_{B(c.n.=6)}$	$T_{order-disorder}$	References
$Gd_2Zr_2O_7$	$Gd^{3+}/Zr^{4+}=1.384$	1,530 °C	[4, 5]
$Sm_2Zr_2O_7$	$Sm^{3+}/Zr^{4+}=1.419$	2,200 °C	[4]
$Nd_2Zr_2O_7$	$Nd^{3+}/Zr^{4+}=1.454$	2,300 °C	[4]

Table 2 Melting temperatures and R_A/R_B ratio for $Ln_2Ti_2O_7$

Compounds	$R_{A(c.n.=8)}/R_{B(c.n.=6)}$	$T_{melting}$
$Lu_2Ti_2O_7$	$Lu^{3+}/Ti^{4+}=1.493$	1,960 °C
$Yb_2Ti_2O_7$	$Yb^{3+}/Ti^{4+}=1.507$	1,890 °C
$Tm_2Ti_2O_7$	$Tm^{3+}/Ti^{4+}=1.507$	1,820 °C
$Gd_2Ti_2O_7$	$Gd^{3+}/Ti^{4+}=1.6$	1,740 °C

The basic mechanism of oxygen transport in the pyrochlore structure is O^{2-} ion hopping; a continuous and energetically favorable pathway is 48f⟺48f position jumps [6]. In the ideal fluorite structure such an energetically preferential process cannot be realized because of the anion disorder. The total strain energy of the lattice (ΔH_σ) at jumps 48f⟺48f for different pyrochlore type structures $A_2B_2O_7$ has been calculated [6, 7]. For rare-earth element titanates with small radii ($Lu_2Ti_2O_7$, $Yb_2Ti_2O_7$, $Tm_2Ti_2O_7$) the calculated lattice total strain energy ΔH_σ was the lowest among all rare-earth titanates and was the same as ΔH_σ for $Gd_2Zr_2O_7$ (~40 a.u.) [6].

In this paper, following the theoretical prediction [6], we investigated the possibility of the pyrochlore–fluorite transformation in $Ln_2Ti_2O_7$ (Ln = Lu, Yb, Tm) at high temperatures (1,400–1,700 °C). In the course of this study we investigated the behavior of coprecipitation products Ln:Ti = 1:1 (Ln = Lu, Yb, Tm) in the wide temperature range 350–1,700 °C.

Experimental

Ln^{3+} and Ti^{4+} hydroxides were coprecipitated in the stoichiometric ratio Ln^{3+}:Ti^{4+} = 1:1 from Ln^{3+} and Ti^{4+} chloride solutions by adding ammonium hydroxide at pH = 11. Then they were separated from the solution by centrifuge and washed with distilled hot water several times to remove the chloride ions. The residues were frozen and freeze-dried ($P = 5{\cdot}10^{-2}$mbar, $T = -30$ to $+30$ °C, $t = 48$ h). The further heat treatment of as-obtained precursors was performed by annealing in air at 650, 740, 800, 850, 950, 1,400, and 1,700 °C. Ceramic samples were prepared in two stages: annealing of the coprecipitation products at 740 °C, pressing them at 100 kg/cm^2 into pellets, and second annealing at the higher temperatures of 950, 1,400, and 1,700 °C. The characteristics of all the synthesized samples are presented in Table 3. The control of the composition of ceramics was performed by mass spectrometry (EMAL-2 mass spectrometer). XRD (X-ray diffraction analysis) of the powder and ceramic samples was carried out using a DRON-3 M automatic diffractometer (Cu K_α) operating at 35 kV and 28 mA. Diffraction data were collected in the 2θ range from 15 to 45° or 65°, counting for 3 s at each 0.1° 2θ step. Rietveld refinement was performed using XRD patterns (Cu K_α, 2Θ = 10–80°, step 0.05°, 3 s/step) of powders obtained by grinding of the ceramic samples. Fullprof software [8] was used for the structure refinement. The conductivity of ceramic samples was tested by a two-probe method using a balance bridge (TESLA BM 431E) at the frequency of 1 MHz in the temperature range 350–950 °C. For electrical measurements ceramic specimens were painted with Pt paste and fired at 1,000 °C. Microstructural observations of sintered samples were performed by scanning electron microscope (SEM). Thermogravimetric and thermal analyses (TGA, DTA) were performed in air with a SETARAM TG-DTA-92 at a heating rate of 20°/min.

Results and discussion

The thermal analysis data of freeze-dried coprecipitation products with cation ratio Ln:Ti = 1:1 (Ln = Lu, Yb, Tm) show sharp exothermic maxima at 750–820 °C; mass loss takes place up to 1,000 °C (Fig. 1).

Figures 2, 3 and 4 illustrate the phase formation process for $Lu_2Ti_2O_7$, $Yb_2Ti_2O_7$, and $Tm_2Ti_2O_7$, respectively, at moderate temperatures (650–950 °C). As one can see, the existence of the fluorite phases at 650–740 °C is observed for $Ln_2Ti_2O_7$ in all three cases. The formation of the low-temperature fluorite polymorph was also confirmed by IR spectroscopy (Fig. 5). IR spectra of all these samples exhibit full absence of the pyrochlore structure absorption bands at 310, 380, and 610 cm^{-1}. At $T > 800$ °C the disordered pyrochlore structure with antisite cation and anion defects is formed, as confirmed

Table 3 Characteristics of the samples

Sample	Thermal processing scheme	Characteristic
No 1 $Lu_2Ti_2O_7$	740 °C (2 h), 950 °C (10 h), 650 °C (100 h)	White, low density (46%)
No 2 $Lu_2Ti_2O_7$	740 °C (2 h), 950 °C (10 h)	White, low density (46.5%)
No 3 $Lu_2Ti_2O_7$	740 °C (2 h), 1,400 °C (10 h)	Orange, transparent, density 92.5%
No 4 $Lu_2Ti_2O_7$	740 °C (2 h), 1,700 °C (10 h)	Brown, transparent, density 93%
No 5 $Yb_2Ti_2O_7$	740 °C (2 h), 950 °C (10 h), 650 °C (100 h)	White, low density (51.5%)
No 6 $Yb_2Ti_2O_7$	740 °C (2 h), 950 °C (10 h)	White, low density (52%)
No 7 $Yb_2Ti_2O_7$	740 °C (2 h), 1,400 °C (10 h)	Light-yellow, transparent, density 92.5%
No 8 $Yb_2Ti_2O_7$	740 °C (2 h), 1,700 °C (10 h)	Pinkish, transparent, density 93%
No 9 $Tm_2Ti_2O_7$	740 °C (2 h), 950 °C (10 h), 650 °C (100 h)	White, low density (50.5%)
No 10 $Tm_2Ti_2O_7$	740 °C (2 h), 950 °C (10 h)	White, low density (51%)
No 11 $Tm_2Ti_2O_7$	740 °C (2 h), 1,400 °C (10 h)	Light green, transparent, density 92.5%
No 12 $Tm_2Ti_2O_7$	740 °C (2 h), 1,700 °C (10 h)	Olive, transparent, density 93%

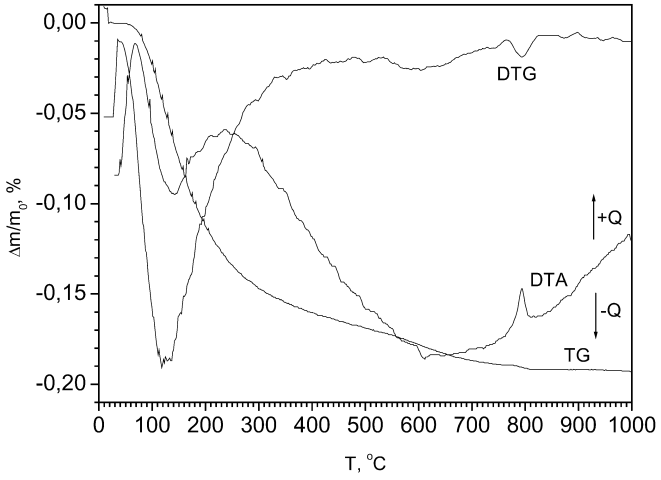

Fig. 1 DTA, DTG, and TG data for freeze-dried coprecipitation product for Lu:Ti = 1:1

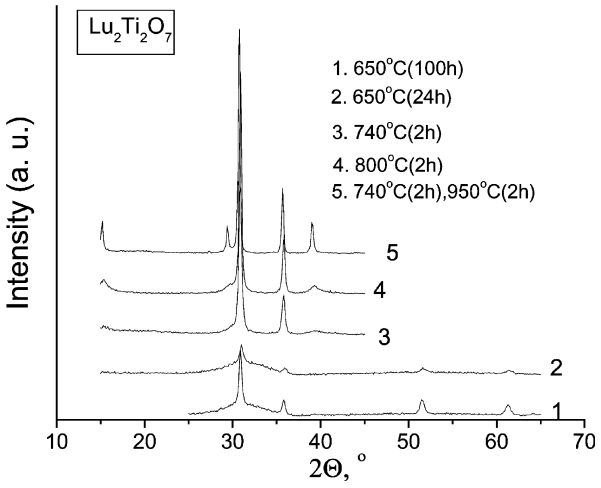

Fig. 2 X-ray diffraction patterns for freeze-dried coprecipitation product Lu:Ti = 1:1, annealed at 650–950 °C

by Rietveld analysis data for $Lu_2Ti_2O_7$ (Table 4). Therefore, the exothermic maxima at $T \sim 750$–820 °C on DTA curves deal with fluorite–pyrochlore transition.

More detailed investigation of the order–disorder transformation in $Lu_2Ti_2O_7$ was performed by Rietveld analysis (Table 4). Lower annealing temperatures of ~850 °C provide the synthesis of $Lu_2Ti_2O_7$ with a pyrochlore structure containing the antisite defects (18–19% Lu–Ti exchange, samples 1 and 3). The Rietveld plot for sample 1 is shown in Fig. 6. At 1,050 °C the antisite defect number is decreased to 6% (sample 2).

Thus, the fluorite phase exists at 600–740 °C, then it converts to a phase with the pyrochlore structure containing cation and anion defects at 740–1,050 °C. The phase $Lu_2Ti_2O_7$, with a perfect pyrochlore structure, forms at $T > 1{,}050$ °C.

It is known that antisite defect formation can be accompanied by the appearance of Frenkel defects in the oxygen sublattice and by the growth of the ionic conductivity contribution [2]. Figures 7 and 8 demonstrate the conductivity data for $Ln_2Ti_2O_7$ (Ln = Lu, Yb, Tm) obtained at different annealing temperatures. Measurements were made in the 350–950 °C temperature range. The conductivity curves for samples thermally treated at 950 and 1,400 °C (Figs. 7, 8; curves 2, 3) are identical in spite of significant difference in the density and color of these samples (Table 3). A change of the slope value of the conductivity curves was observed at 1,000 K (737 °C) (Figs. 7, 8; curves 2, 3).

It is known [9] about the existence of the low-temperature phase at 500–800 °C for $Gd_2Zr_2O_7$ obtained by the coprecipitation method. The high-temperature

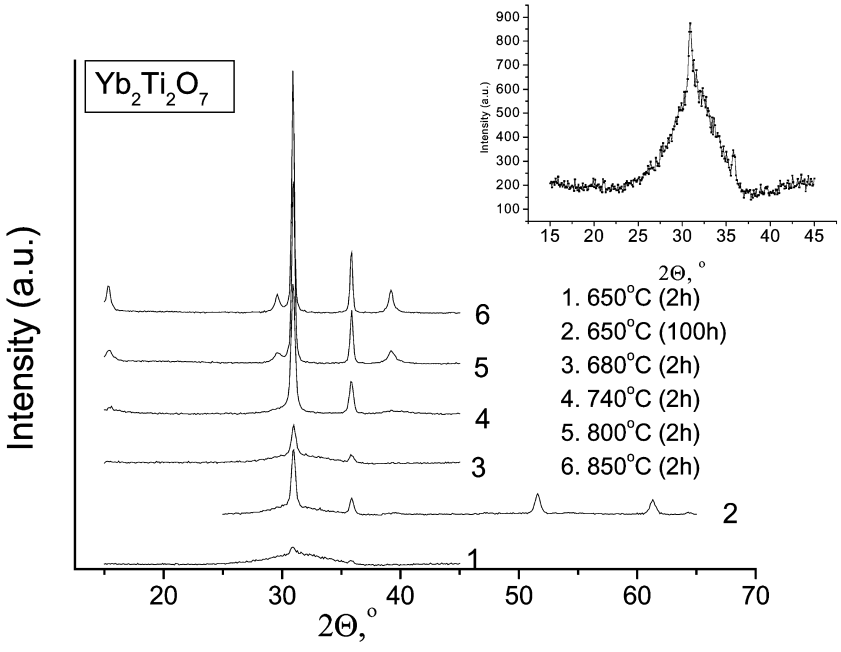

Fig. 3 XRD patterns for freeze-dried coprecipitation product Yb:Ti = 1:1, annealed at 650–850 °C. *Inset*: the peak, related to the fluorite phase, at pattern 1 (650 °C, 2 h)

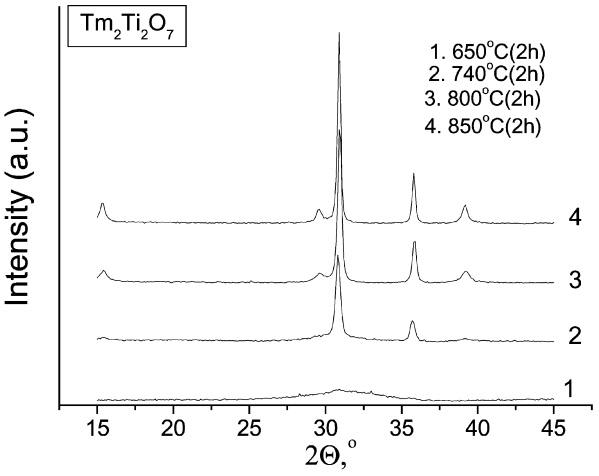

Fig. 4 X-ray diffraction patterns for freeze-dried coprecipitates Tm:Ti = 1:1, annealed at 650–850 °C

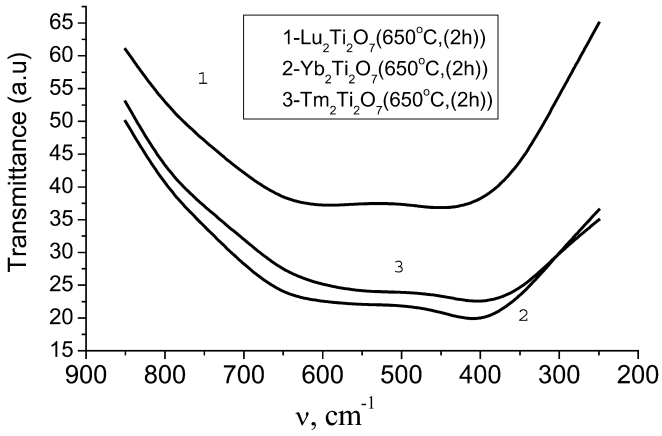

Fig. 5 IR absorption spectra of $Ln_2Ti_2O_7$ (650 °C, 2 h): *1* $Lu_2Ti_2O_7$, *2* $Yb_2Ti_2O_7$, *3* $Tm_2Ti_2O_7$

pyrochlore–fluorite transformation for $Gd_2Zr_2O_7$ at $T > 1{,}530$ °C has also been reported [4, 5]. Taking into account almost the same ΔH_σ values for $Gd_2Zr_2O_7$ and $Ln_2Ti_2O_7$ (Ln = Lu, Yb, Tm) [6], we investigated the behavior of $Ln_2Ti_2O_7$ at 1,400–1,700 °C in order to detect possible pyrochlore–fluorite transformations.

The pyrochlore structure is distinguished from fluorite by ordering of the cations in the 16d (1/2,1/2,1/2) and 16c (0,0,0) sites, and by the displacement of 48f oxygen along the *X*-axis. In the XRD patterns this difference causes additional reflections, namely 311 (2Θ∼29.5°) and 331 (2Θ∼39°). Figures 9a–c show X-ray patterns for samples $Tm_2Ti_2O_7$, $Yb_2Ti_2O_7$, and $Lu_2Ti_2O_7$ annealed at 1,400 and 1,700 °C. A considerable decrease of the 311 and 331 line intensities is observed for pyrochlore $Tm_2Ti_2O_7$ annealed at 1,700 °C in comparison with the sample annealed at 1,400 °C (Fig. 9a). Rietveld analysis demonstrated the absence of antisite defects. Annealing at 1,700 °C (Fig. 7, curve 1) also changes the character of the conductivity curve for $Tm_2Ti_2O_7$ at 650–1,400 °C (Fig. 7, curves 2, 3). The conductivity level for $Tm_2Ti_2O_7$, obtained at 1,700 °C, was considerably higher than that for the other samples, and the change of the slope at 737 °C disappeared. Linear and monotonous dependence of $\log\sigma$ on $1/T$ at 350–950 °C shows in the single transport mechanism for this sample through the whole temperature range studied. We attribute these changes to the high-temperature pyrochlore–fluorite transformation at $T \sim 1{,}700$ °C. The same transformations were also observed for $Yb_2Ti_2O_7$ and $Lu_2Ti_2O_7$ at 1,700 °C.

Figure 9b demonstrates the changes in the pyrochlore structure of $Yb_2Ti_2O_7$ at 1,400–1,700 °C. The decrease of the 311 and 331 line intensities usually reflects the transformation of pyrochlore to fluorite. In $Yb_2Ti_2O_7$ samples annealed at 1,700 °C, the lines 311 and 331 are smaller than those for the same ceramics annealed at 1,400 °C, which indicates the beginning of high-temperature order–disorder transformation. Figure 8

Table 4 Structure refinement results for $Lu_2Ti_2O_7$ ceramics

Thermal schedule	Parameter (Å)	Element	Occupancy	*X*	*Y*	*Z*	R_{wp} (%)
No. 1: 850 °C (2 h), 860 °C (1 h), quench to liquid N_2	10.002(1)	Lu (Lu)	0.818(3)	0.625	0.625	0.625	$R_{wp} = 10.97$
		Ti (Lu)	0.182	0.625	0.625	0.625	
		Ti (Ti)	0.818	0.125	0.125	0.125	
		Lu (Ti)	0.182	0.125	0.125	0.125	
		O (O1)	1	0.5	0.5	0.5	
		O (O2)	1	0.20161	0	0	
No. 2: 850 °C (2 h), 1,050 °C (1 h), quench to liquid N_2	9.998(1)	Lu (Lu)	0.933(3)	0.625	0.625	0.625	$R_{wp} = 10.61$
		Ti (Lu)	0.067	0.625	0.625	0.625	
		Ti (Ti)	0.933	0.125	0.125	0.125	
		Lu (Ti)	0.067	0.125	0.125	0.125	
		O (O1)	1	0.5	0.5	0.5	
		O (O2)	1	0,1931	0	0	
No. 3: 850 °C (2 h), 860 °C (1 h), quench to N_2, +740 °C (48 h)	10.024(1)	Lu (Lu)	0.807(4)	0.625	0.625	0.625	$R_{wp} = 11.91$
		Ti (Lu)	0.193	0.625	0.625	0.625	
		Ti (Ti)	0.807	0.125	0.125	0.125	
		Lu (Ti)	0.193	0.125	0.125	0.125	
		O (O1)	1	0.5	0.5	0.5	
		O (O2)	1	0.19693	0	0	

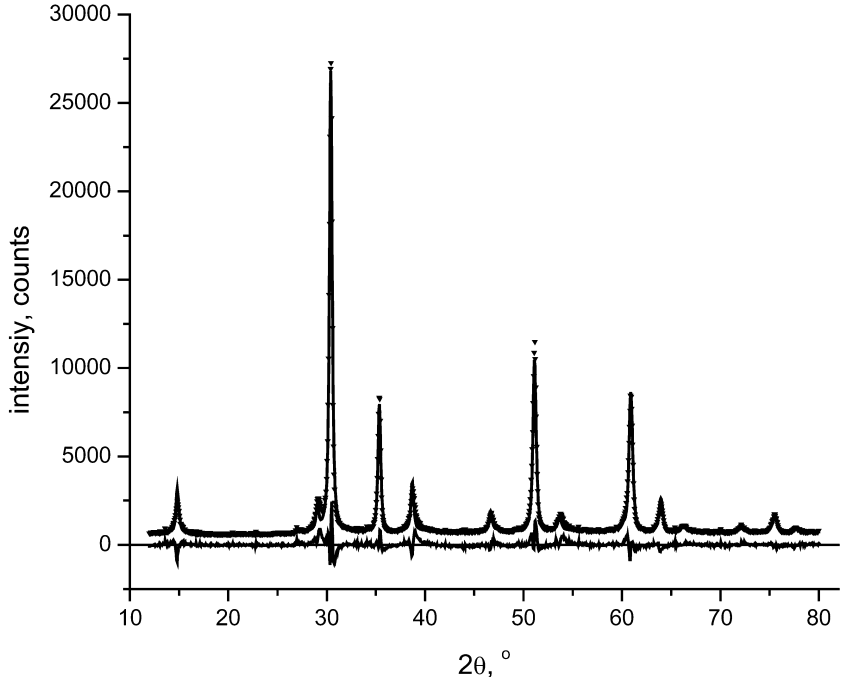

Fig. 6 Rietveld plot for $Lu_2Ti_2O_7$ (sample 1): 850 °C (2 h), 860 °C (1 h), quench to liquid N_2

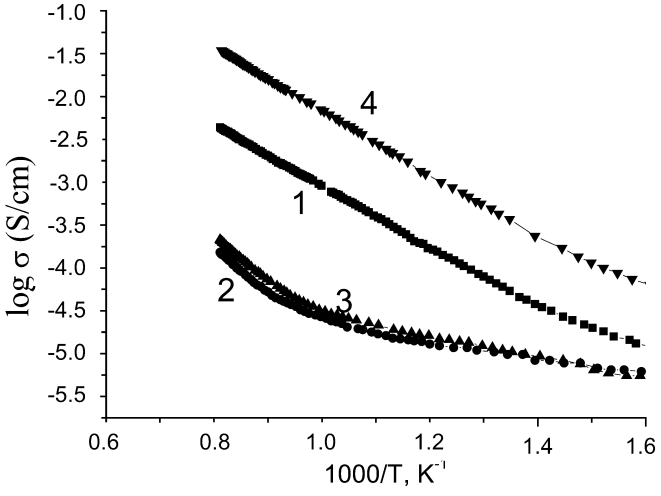

Fig. 7 The temperature dependence of the electrical conductivity for $Tm_2Ti_2O_7$ and $Lu_2Ti_2O_7$, annealed at different temperatures: *1*$Tm_2Ti_2O_7$, 740 °C (2 h), 1,700 °C (10 h); *2*$Tm_2Ti_2O_7$, 740 °C (2 h), 1,400 °C (10 h); *3*$Tm_2Ti_2O_7$, 740 °C (2 h), 950 °C (10 h); *4*$Lu_2Ti_2O_7$, 740 °C (2 h), 1,700 °C (10 h)

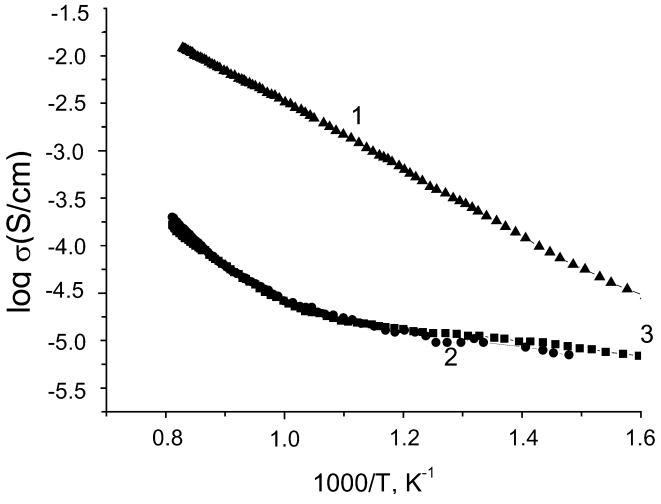

Fig. 8 The temperature dependence of the electrical conductivity for $Yb_2Ti_2O_7$, annealed at different temperatures: *1*$Yb_2Ti_2O_7$, 740 °C (2 h), 1,700 °C (10 h); *2*$Yb_2Ti_2O_7$, 740 °C (2 h), 1,400 °C (10 h); *3*$Yb_2Ti_2O_7$, 740 °C (2 h), 950 °C (10 h)

(curve 1) displays the conductivity growth in $Yb_2Ti_2O_7$ ceramics, annealed at 1,700 °C, in comparison with the conductivity values observed in other $Yb_2Ti_2O_7$ samples (950–1,400 °C) (Fig. 8, curves 2, 3). Figure 9c demonstrates the XRD patterns of $Lu_2Ti_2O_7$ obtained at 1,400 °C and 1,700 °C. The decrease of intensities of the 311 and 331 lines for $Lu_2Ti_2O_7$, annealed at 1,700 °C, was accompanied by significant conductivity growth (Fig. 7, curve 4).

The electrical conductivity of the rare-earth titanates $Ln_2Ti_2O_7$ was measured for the first time by Brixner [10]. The conductivity of $Ln_2Ti_2O_7$ (Ln = La–Lu) was determined using the DC method. Unfortunately, the conductivity data for $Ln_2Ti_2O_7$ (Ln = Lu, Yb, Tm) [10] were presented only at 25 °C. It should be noted also that the $Ln_2Ti_2O_7$ (Ln = La–Lu) were prepared by the solid-state synthesis method at 1,200–1,650 °C (14 h). We used a coprecipitation method that provides the synthesis of the fluorite phases at 600–740 °C. According to Brixner [10], $Ln_2Ti_2O_7$ (Ln = Sm, Ho, Er) has p-type conductivity (E_a~1.98 eV for $Er_2Ti_2O_7$) at high temperatures in the range 700–950 °C. The conductivity of $Ln_2Ti_2O_7$

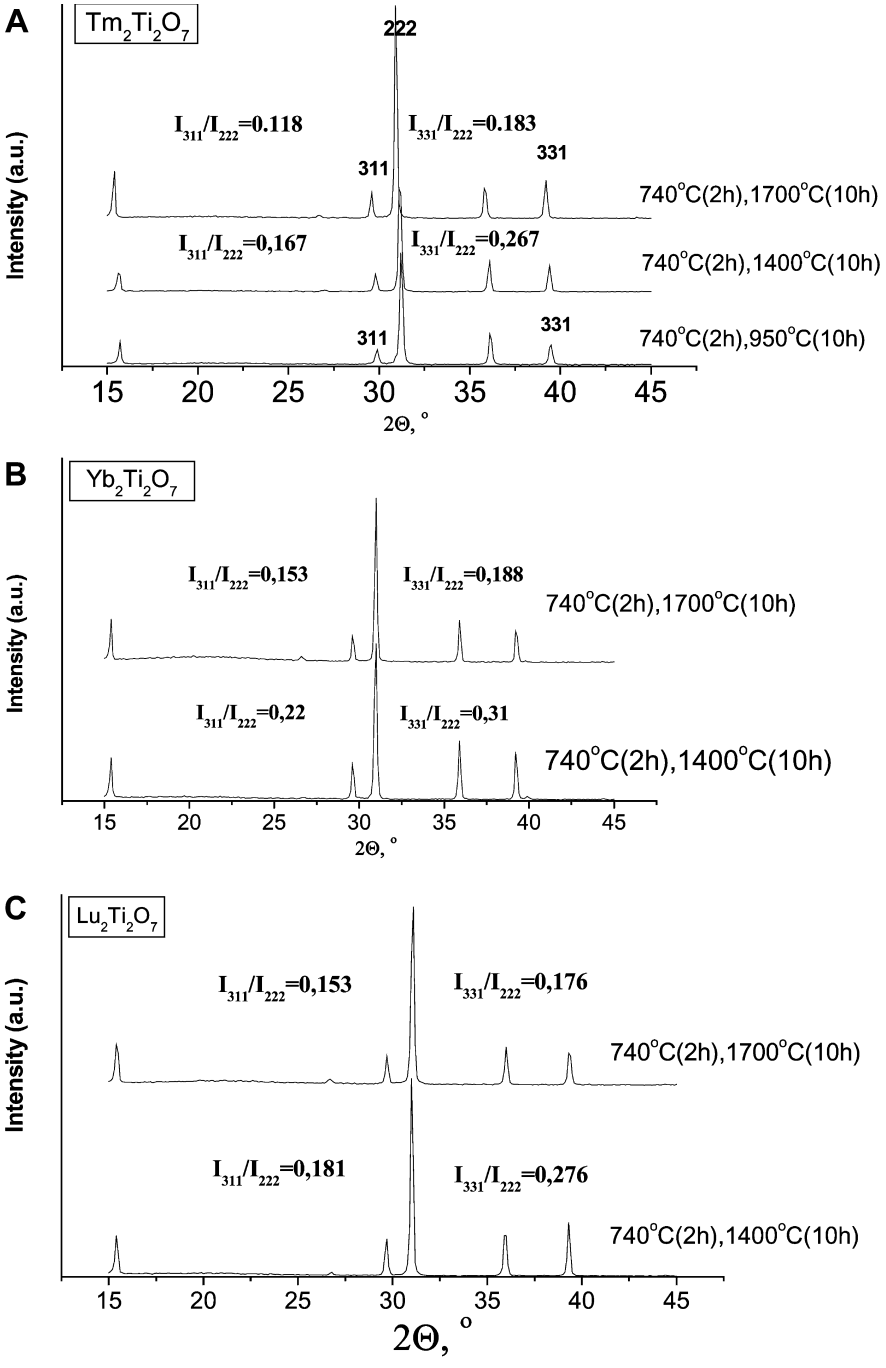

Fig. 9 a XRD patterns for $Tm_2Ti_2O_7$, annealed at high temperatures. **b** XRD patterns for$Yb_2Ti_2O_7$, processed at 1,400 °C and 1,700 °C. **c** XRD patterns for $Lu_2Ti_2O_7$, processed at 1,400 °C and 1,700 °C

(Ln = Lu, Yb, Tm) samples, studied in the present work, at 700–950 °C cannot be considered as essentially electronic (E_a~0.71 eV for $Lu_2Ti_2O_7$, E_a~0.64 eV for $Yb_2Ti_2O_7$, and E_a~0.66 eV for $Tm_2Ti_2O_7$). Figure 10 shows the microstructure for one of our $Lu_2Ti_2O_7$ samples (740 °C (2 h), 950 °C (2 h)). The grain size for this ceramic is proved to be 13–15 nm. These conductivity results can be connected with both a high Frenkel anion defect concentration in pyrochlore $Ln_2Ti_2O_7$ and the outstandingly small grain size of our samples compared to the coarse-grained ceramics measured previously [10].

Conclusions

For the first time the low-temperature fluorite–pyrochlore transition in $Ln_2Ti_2O_7$ (Ln: rare-earth cations with small radii) was observed at ~740–800 °C. Low-temperature fluorites have been obtained by coprecipitation followed by freeze-drying and thermal decomposition of the salt precursor. The region of the low-temperature fluorite phase existence is 600 °C < T < 740 °C. At T > 800 °C, $Ln_2Ti_2O_7$ (Ln = Lu, Yb, Tm) have the

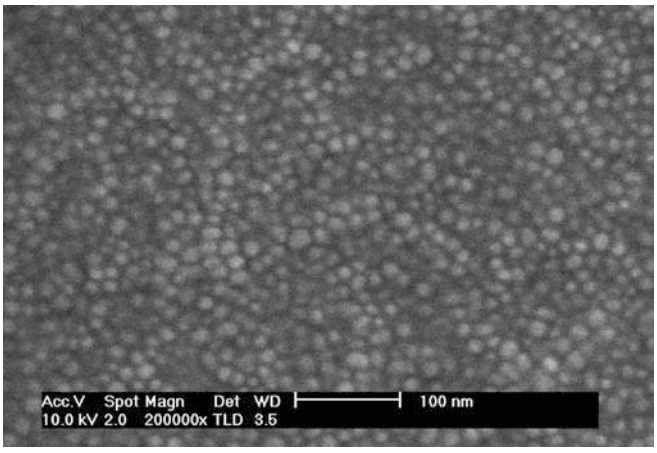

Fig. 10 SEM micrograph of $Lu_2Ti_2O_7$ ceramics: 740 °C (2 h), 950 °C (10 h)

structure of disordered pyrochlore with antisite Ln–Ti defects and Frenkel oxygen defects. $Ln_2Ti_2O_7$ (Ln = Lu, Yb, Tm) with the perfect pyrochlore structure exist at 1050 °C < T < 1600 °C. The high-temperature pyrochlore–fluorite transformation, observed in $Yb_2Ti_2O_7$, $Tm_2Ti_2O_7$, and $Lu_2Ti_2O_7$ at $T > 1600$ °C, is connected with Frenkel oxygen defects in the pyrochlore structure. The order–disorder transformation at 1,700 °C is accompanied by the growth of the conductivity values for 2 orders of magnitude.

Acknowledgements The authors gratefully acknowledge Ms. Elena Kharitonova from the Moscow State University (Physical Department) for conductivity measurements of samples. This work was financially supported by the Russian Foundation for Basic Research (grant no. 01-03-33315).

References

1. Tuller HL, Kramer SA, Spears MA, Pal UB (1996) US Patent 5,509,189
2. Eberman KW, Wuensch BJ, Jorgensen JD (2002) Solid State Ionics 148:521
3. Moon PK, Tuller HL (1990) Sens Actuators B Chem 1:199
4. Michel D, Perez y Jorba M, Collongues R (1974) Mater Res Bull 9:1457
5. Meilicke S, Haile S (1995) Mater Res Soc Symp Proc 135:55
6. van Dijk MP, de Vries KJ, Burggraaf AJ (1983) Solid State Ionics 9/10:913
7. Dell RM, Hooper A (1978) In: Hagenmuller P, Van Gool W (eds) Solid electrolytes. Academic, New York, p 291
8. Izumi F (1993) In: Yong RA (ed) The Rietveld method. Oxford University Press, Oxford
9. Fomina LN, Palguev SF (1977) Zh Neorg Khim 22:326
10. Brixner LH (1964) Inorg Chem 3:1065